Article

A Hybrid Quantum Dot–Antibody Fragment Fluorescence Resonance Energy Transfer-Based TNT Sensor

Ellen R. Goldman, Igor L. Medintz, Jessica L. Whitley, Andrew Hayhurst, Aaron R. Clapp, H. Tetsuo Uyeda, Jeffrey R. Deschamps, Michael E. Lassman, and Hedi Mattoussi

J. Am. Chem. Soc., **2005**, 127 (18), 6744-6751• DOI: 10.1021/ja043677l • Publication Date (Web): 13 April 2005

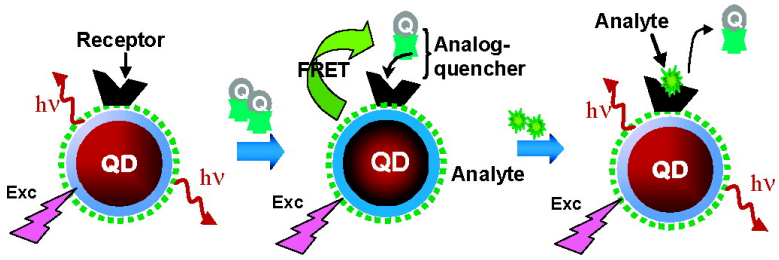

More About This Article

Additional resources and features associated with this article are available within the HTML version:

- Supporting Information
- Links to the 24 articles that cite this article, as of the time of this article download
- Access to high resolution figures
- Links to articles and content related to this article
- Copyright permission to reproduce figures and/or text from this article

View the Full Text HTML

J|A|C|S
ARTICLES
Published on Web 04/13/2005

A Hybrid Quantum Dot−Antibody Fragment Fluorescence Resonance Energy Transfer-Based TNT Sensor

Ellen R. Goldman,*,† Igor L. Medintz,† Jessica L. Whitley,‡ Andrew Hayhurst,§ Aaron R. Clapp,§ H. Tetsuo Uyeda,¶ Jeffrey R. Deschamps,# Michael E. Lassman,† and Hedi Mattoussi*,¶

Contribution from the Center for Bio/Molecular Science and Engineering, U.S. Naval Research Laboratory, Washington, D.C. 20375, The Center for Biomedical Genomics, George Mason University, Fairfax, Virginia 22030, Department of Virology and Immunology, Southwest Foundation for Biomedical Research, 7620 N.W. Loop 410, San Antonio, Texas 78227-5301, Division of Optical Sciences, U.S. Naval Research Laboratory, Washington, D.C. 20375, and Laboratory for the Structure of Matter, U.S. Naval Research Laboratory, Washington, D.C. 20375

Received October 18, 2004; E-mail: erg@cbmse.nrl.navy.mil (E.R.G); hedimat@ccs.nrl.navy.mil (H.M.)

Abstract: We demonstrate the use of luminescent QDs conjugated to antibody fragments to develop solution-phase nanoscale sensing assemblies, based on fluorescence resonance energy transfer (FRET) for the specific detection of the explosive 2,4,6-trinitrotoluene (TNT) in aqueous environments. The hybrid sensor consists of anti-TNT specific antibody fragments attached to a hydrophilic QD via metal-affinity coordination. A dye-labeled TNT analogue prebound in the antibody binding site quenches the QD photoluminescence via proximity-induced FRET. Analysis of the data collected at increasing dye-labeled analogue to QD ratios provided an insight into understanding how the antibody fragments self-assemble on the QD. Addition of soluble TNT displaces the dye-labeled analogue, eliminating FRET and resulting in a concentration-dependent recovery of QD photoluminescence. Sensor performance and specificity were evaluated.

Introduction

Detection of 2,4,6-trinitrotoluene (TNT) and other derivative explosives in aqueous environments (including seawater) has become a current priority. Long-term manufacturing of explosives and cumulative use of land and marine firing ranges, as well as military conflicts, have all resulted in severe contamination from unexploded ordnance and mines worldwide.[1−4] Exposure to these compounds is toxic to many organisms ranging from plants and fungi to humans.[5,6] Contaminated areas need to be identified, monitored, and ultimately remediated. More recently, global security concerns have dictated a need for port and naval detection of undersea explosives.[7,8] Consequently, there is a pressing need for detection technologies to be developed for long-term monitoring in these challenging environments.

The unique properties of luminescent colloidal semiconductor nanocrystals (quantum dots, QDs) suggest they may be particularly well suited for use in optically based detection schemes in aqueous environments. QD properties of interest include exceptional resistance to photo- and chemical degradation, broad absorption spectra with size-tunable narrow, symmetric photoluminescent (PL) spectra (full width at half max ∼25−40 nm) spanning from the UV to near-IR with high quantum yields, and achievable large Stokes shifts.[9−11] Although QDs have been used extensively in a variety of bio-inspired applications,[9−13] their properties have only recently been exploited in an active sensing modality.

We have recently used CdSe−ZnS core−shell nanocrystals conjugated to dye-labeled proteins to demonstrate that QDs are excellent energy donors and nanoscaffolds in fluorescence

† Center for Bio/Molecular Science and Engineering, U.S. Naval Research Laboratory.
‡ George Mason University.
§ Southwest Foundation for Biomedical Research.
¶ Division of Optical Sciences, U.S. Naval Research Laboratory.
# Laboratory for the Structure of Matter, U.S. Naval Research Laboratory.

(1) Spaulding, R. F.; Fulton, J. W. *J. Contam. Hydrol.* **1988**, *2*, 139−153.
(2) Charles, P. T.; Dingle, B. M.; Van Bergen, S.; Gauger, P. R.; Patterson, C. H.; Kusterbeck, A. W. *Field Anal. Chem. Technol.* **2001**, *5*, 272−280.
(3) Boopathy, R.; Manning, J.; Montemagno, C.; Rimkus, K. *Can. J. Microbiol.* **1994**, *40*, 787−790.
(4) Darrach, M. R.; Chutjian, A.; Plett, G. A. *Environ. Sci. Technol.* **1998**, *32*, 1354−1358.
(5) Won W. D.; Disalvo, L. H.; Ng, J. *Appl. Environ. Microbiol*. **1976**, *31*, 576−580.
(6) Kaplan, D. L.; Kaplan, A. M. *Environ. Sci. Technol*. **1982**, *16*, 566−571.
(7) D'Amico, E. *Chem. Week* **2002**, *164*, 25−26.
(8) Makrinos, S. T. *Sea Technol*. **2004**, *45*, 33−34.
(9) Murphy, C. J. *Anal. Chem*. **2002**, *74*, 520A−529.
(10) Parak, W. J.; Gerion, D.; Pellegrino, T.; Zanchet, D.; Micheel, C.; Williams, S. C.; Boudreau, R.; Le Gros, M. A.; Larabell, C. A.; Alivisatos, A. P. *Nanotechnology* **2003**, *14*, R15−R27.
(11) Mattoussi, H.; Kuno, M. K.; Goldman, E. R.; Anderson, G. P.; Mauro, J. M. Colloidal Semiconductor Quantum Dot Conjugates in Biosensing. In *Optical Biosensors: Present and Future*; Ligler, F. S., Rowe Taitt, C. A., Eds.; Elsevier Science: New York, 2002; Chapter 17.
(12) Goldman, E. R.; Balighian, E. D.; Mattoussi, H.; Kuno, M. K.; Mauro, J. M.; Tran, P. T.; Anderson, G. P. *J. Am. Chem. Soc.* **2002**, *124*, 6378−6382.
(13) Goldman, E. R.; Anderson, G. P.; Tran, P. T.; Mattoussi, H.; Charles, P. T.; Mauro, J. M. *Anal. Chem*. **2002**, *74*, 841−847.

10.1021/ja043677l CCC: $30.25

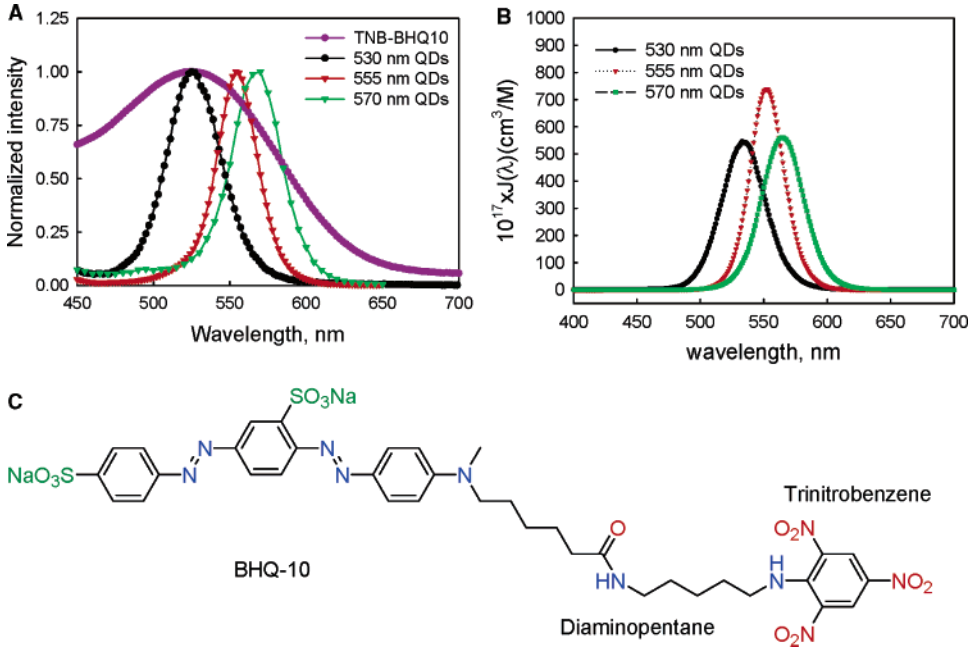

Figure 1. (A) Normalized absorption spectra of TNB−DAP−BHQ-10 (TNB−BHQ-10) plotted together with the normalized fluorescence spectra of QDs used in this study. (B) Spectral overlap functions defined as $J(\lambda) = PL_{D-corr}(\lambda) \times \lambda^4 \times \epsilon_A(\lambda)$ for the three QD donor−BHQ-10 acceptor pairs plotted versus wavelength. The Förster distance, R_0, at which the energy transfer efficiency reaches 50%, estimated using the experimental overlap integral, is ∼43, ∼45.9, and ∼42.2 Å for the 530, 555, and 570 nm emitting QDs, respectively.[14,32] (C) Chemical structure of the TNB−BHQ-10 quencher analogue.

resonance energy transfer (FRET) assays and sensors with organic dye acceptors.[14,15] In these studies, maltose binding protein (MBP) was self-assembled onto the nanocrystals, via metal-affinity coordination employing a protein expressing an oligohistidine sequence, to provide aggregate-free solutions of QD−MBP conjugates. These conjugates were used to assemble a solution-phase sensor specific for maltose. In this prototype sensor, the MBP was prelabeled with a sugar dye analogue in its central binding pocket, which quenched QD PL due to proximity-induced FRET. Addition of the target analyte, in this case, the nutrient maltose, resulted in displacement of the sugar dye analogue and manifested in a concentration-dependent recovery in QD PL.[15] The flexibility in choosing the excitation line anywhere below the first absorption peak of the nanocrystals combined with the narrow excitation spectra of dyes permits excitation of the assembly at the dye absorption minimum, thus reducing unwanted direct excitation of the acceptor while realizing efficient FRET. Further examination of QD−FRET interactions demonstrated two specific benefits of this configuration which are not realizable when using conventional organic fluorophores; QD PL can be size-tuned to improve spectral overlap with a particular acceptor, and having several acceptors interact with a single QD donor substantially improves FRET efficiency.[14,15] These features were confirmed by steady-state and time-resolved fluorescence measurements.[14,15]

In the current work, we extend our sensor design beyond the initial prototype and demonstrate a self-assembled QD-based FRET sensor for the detection of 2,4,6-trinitrotoluene (TNT). The sensor consists of anti-TNT specific antibody fragments (single-chain Fv fragments, scFvs), appended with an oligohistidine sequence, specifically immobilized on the surface of CdSe−ZnS QDs. The use of an antibody fragment instead of a full antibody provides a more compact QD conjugate and is better suited for FRET, as distances between donor and antibody-bound acceptor are substantially reduced. A dye-labeled TNT analogue prebound in the scFv binding/recognition site quenches the QD PL via proximity-induced FRET. Addition of TNT to the solution displaces the dye-labeled analogue and results in a concentration-dependent recovery of the QD PL signal. Various TNT analogues and samples originating from TNT-contaminated soil were tested against the sensor to determine sensitivity and specificity.

Experimental Section

QD Synthesis. CdSe−ZnS core−shell QDs with emission maxima at three wavelengths (530, 555, and 570 nm) were selected for the present study because of their favorable spectral overlap with the Black Hole Quencher-10 (BHQ-10, Biosearch Technologies, Novato, CA) used as the energy acceptor for the present FRET investigations (Figure 1A). The corresponding overlap function and the Förster distance (corresponding to a FRET efficiency of 50%) are provided in Figure 1. The nanocrystals were prepared using documented synthetic methods.[16−19] Before use, the nanocrystals were made hydrophilic by exchanging the native capping shell with dihydrolipoic acid (DHLA) ligands, as previously described.[20]

Synthesis and Purification of TNT Analogue Labeled with a Quenching Dye. The dye acceptor used in the present study is a quencher fluorophore with a rather broad excitation spectrum. Its relatively broad absorption allows for strong energy overlap with several

(14) Clapp, A. R.; Medintz, I. L.; Mauro, J. M.; Fisher, B.; Bawendi, M. G.; Mattoussi, H. *J. Am. Chem. Soc.* **2004**, *126*, 301−310.
(15) Medintz, I. L.; Clapp, A. R.; Mattoussi, H.; Goldman, E. R.; Fisher, B.; Mauro, J. M. *Nat. Mater.* **2003**, *2*, 630−638.
(16) Murray, C. B.; Norris, D. J.; Bawendi, M. G. *J. Am. Chem. Soc.* **1993**, *115*, 8706−8715.
(17) Hines, M. A.; Guyot-Sionnest, P. *J. Phys. Chem.* **1996**, *100*, 468−471.
(18) Dabbousi, B. O.; Rodriguez-Viejo, J.; Mikulec, F. V.; Heine, J. R.; Mattoussi, H.; Ober, R.; Jensen, K. J.; Bawendi, M. G. *J. Phys. Chem. B* **1997**, *101*, 9463−9475.
(19) Qu, L.; Peng, Z. A.; Peng, X. *Nano Lett.* **2001**, *1*, 333−337.
(20) Mattoussi, H.; Mauro, J. M.; Goldman, E. R.; Anderson, G. P.; Sundar, V. C.; Mikulec, F. V.; Bawendi, M. G. *J. Am. Chem. Soc.* **2000**, *122*, 12142−12150.

QD donors (see Figure 1). Preparation of the quencher-labeled analogue was carried out as follows; 5 mg of Black Hole Quencher-10 (BHQ-10, Figure 1C) functionalized with a carboxylic acid−succinimidyl ester (Biosearch Technologies, Novato, CA) was dissolved in 50 μL of DMSO and added to 200 mg of 1,5-diaminopentane dihydrochloride (DAP, Sigma-Aldrich, St. Louis, MO) dissolved in 1 mL of 0.136 M Na tetraborate buffer, pH 8.5. The mixed solution was incubated while agitated overnight at room temperature, and then 10% glycerol in 100 μL of HE buffer (10 mM HEPES, 1 mM EDTA buffer, pH 7.0) was added. The solution was separated on a 12% acrylamide 1 × TBE gel. The product bands were excised, and the product was eluted by passive diffusion into HE buffer.[21] The dilute product was concentrated and desalted on an oligonucleotide purification cartridge (OPC, Applied Biosystems, Foster City, CA) as described.[21] Mass spectral analysis was performed on an Applied Biosystems API QSTAR Pulsar Mass Spectrometer by positive electrospray ionization (ESI) to identify the product consisting of the 1:1 monolabeled DAP−BHQ-10. This product was then dissolved in 500 μL of borate buffer, and to this was added 350 μL of 5% 2,4,6-trinitrobenzenesulfonic acid solution (Sigma) mixed with 20 μL of 3 M NaOH. The resulting solution was reacted overnight at room temperature under continuous agitation, loaded on a Supelclean LC-18 SPE column (Supelco, Bellefonte PA), washed with 0.1X borate buffer, and eluted with an increasing concentration of methanol in borate buffer. Eluted fractions were desalted and purified on an OPC column (as above), and the final TNB−DAP−BHQ-10 product (TNB−BHQ-10) was characterized and confirmed with mass spectral analysis.

Protein Expression. The anti-TNT single-chain Fv fragment (TNB2-45), a derivative of TNB2 previously described,[22] was engineered to express a C-terminal $(His)_6GlyGlySerGlyGly(His)_6$, where $(His)_6$ = 6-histidine residue sequence.[22,23] The anti-TNT scFv protein was expressed in the *Escherichia coli* Tuner strain (Novagen, San Diego, CA) and purified from the periplasm as described.[22] Construction and purification of apo-myoglobin protein appended with $(His)_6$ was carried out as described.[23,24]

Assembly of the Antibody-Bound Dye-Labeled Analogue with QDs and FRET Quenching Assays. Five microliters of protein solution (either TNB2-45 or apo-myoglobin, 80 μM stock solutions) and varying amounts of TNB−BHQ-10 reagent (1, 2, 4, 8, 16, and 32 μL of 100 μM stock solution) were mixed together and incubated for 1 h in the dark. Borate buffer (10 mM sodium tetraborate, pH 9) was added to each tube to give a final volume of 115 μL. To these solutions was added 20 μL of QD solution (1.16 μM), and the mix was incubated at room temperature for about 15 min. These solutions were further adjusted by adding 1 mL of borate buffer to each tube to final values of 350 nM for the protein, 20 nM for the QDs, and ranging between ∼88 and ∼2800 nM for the TNB−BHQ-10; 100 μL aliquots of these solutions were transferred into wells of an opaque white microtiter plate (Maxisorb, Nunc, Roskilde, Denmark). These preparations correspond to conjugates with TNB2-45 to QD ratio of ∼17 and a TNB−BHQ-10 (acceptor) to QD (donor) ratio varying approximately between ∼4 and ∼128. Fluorescence spectra were collected on a Tecan Safire plate reader (Tecan US, Research Triangle Park, NC) using 400 nm excitation; when intensities were needed, the PL spectra were integrated over a narrow window (5 nm) around the emission maximum of the QD used. Signals for three triplicate wells were averaged. Controls containing QD−protein conjugates but no TNB−dye were also prepared.

Construction of QD−Protein Conjugate Model. No structural information is available on antigen binding by TNB2-45, on the conformation of TNB−BHQ-10, or on the histidine-rich tail (even though such regions are present in structures deposited with the protein database (PDB)). A model of the QD−protein conjugate was constructed based on the crystal structure of a single-chain Fv (scFv) derived from a phage library and models of TNB−BHQ-10 and the histidine-rich tail. A starting structure was selected based on sequence homology of single-chain antibodies (in the PDB) to the sequence of TNB2. An alignment of the sequences of 1DZB[25] and TNB2 was prepared based on sequence homology and the conserved (invariant) regions of the scFv. Structures of the histidine-rich tail and TNB−BHQ-10 were constructed using Chem-3D Ultra and incorporated into the PDB-derived structure using MidasPlus, which was also used for final rendering.[26,27] TNB−BHQ-10 was docked with the variable region of the scFv model by examining contacts between the antibody and TNB−BHQ-10. Since the binding site in TNB2 is known to recognize TNB and TNT, the docking site was selected to create a $\pi-\pi$ interaction between the scFv and antigen. The histidine-rich tail was folded to allow interaction of the histidine side chains with the QD surface and to match the separation between the QD center and TNB−BHQ-10 with the experimentally measured value.

TNT-Contaminated Soil Samples. Soil samples tested were dry and well-homogenized archived soils taken from Umatilla Army Depot Activity (UMDA), Hermiston, OR and were provided by H. Craig (U.S. EPA, Region 10). We used an acetone-based extraction to retrieve TNT from the soil samples.[28,29] Briefly, extracts were prepared by mixing 2.0 g of soil with 10 mL of acetone in glass vials. Each sample was shaken for 3 min then filtered through a 0.22 μm syringe filter (Nylon Acrodisc, Pall Corp., East Hills, NY). Acetone extracts were stored in the dark at −20 °C prior to analysis. Immediately prior to performing an assay, small volumes of acetone extracts were transferred to glass test tubes, the acetone was evaporated by brief treatment with a stream of nitrogen flow, followed by dissolution in borate buffer. The volume of borate buffer added to the TNT in the test tube was 10 times the volume of the original acetone sample, creating a 1/10 dilution of the TNT in the extract. The TNT concentration in each of these samples was determined by several methods, including HPLC, as previously described.[28,29]

Competition Displacement Assays. First, a working solution made of TNB2-45 (2.96 μM), QDs (172 nM), and TNB−BHQ-10 (5.93 μM) was prepared by incubating the protein and TNB−BHQ-10 in the dark for 1 h, then adding borate buffer and QD solution. After a 15 min incubation, the volume was increased to give final concentrations of TNB2-45 (639 nM), QDs (36.5 nM), and TNB−BHQ-10 (1.26 μM); this corresponds to a TNB2-45 to QD ratio of ∼17 and a TNB−BHQ-10 to QD ratio of ∼34, as described above (QD:TNB2-45:TNB−BHQ-10 = 1:17:34). Fifty microliter aliquots of this solution were added to wells of a microtiter plate. Next, 50 μL of TNT (Cerilliant Corp., Round Rock, TX) dilutions in borate buffer (and buffer only, no TNT controls) were added to appropriate test and control wells. Signal (background-corrected) was plotted as the difference between the fluorescence recorded at each TNT concentration and that collected from wells with no TNT. All measurements were done in triplicate. Detection of the TNT analogues, 2,6-dinitrotoluene (2,6-DNT), 2-amino-4,6-dinitrotoluene (2A-4,6-DNT), and Tetryl (Cerilliant), was as above. Artificial seawater was prepared by dissolving 40 g of sea salts (Sigma) into 1 L of water.

For TNT solutions extracted from soil samples, the assay was carried out as described above; 50 μL aliquots of reagent stock solution (made

(21) Medintz, I. L.; Goldman, E. R.; Lassman, M. E.; Mauro, J. M. *Bioconjugate Chem.* **2003**, *14*, 909−918.
(22) Goldman, E. R.; Hayhurst, A.; Lingerfelt, B. M.; Iverson, B. L.; Georgiou, G.; Anderson, G. P. *J. Environ. Mon.* **2003**, *5*, 380−383.
(23) Goldman, E. R.; Medintz, I. L.; Hayhurst, A.; Anderson, G. P.; Mauro, J. M.; Iverson, B. L.; Georgiou, G.; Mattoussi, H. *Anal. Chim. Acta* **2005**, *524*, 63−67.
(24) Jhaveri, S. D.; Mauro, J. M.; Goldston, H. M.; Schauer, C. L.; Tender, L. M.; Trammell, S. A. *Chem. Commun.* **2003**, *3*, 338−339.
(25) Ay, J.; Keitel, T.; Kuttner, G.; Wessner, H.; Scholz, C.; Hahn, M.; Hohne, W. *J. Mol. Biol.* **2000**, *301*, 239−246.
(26) Ferrin, T. E.; Huang, C. C.; Jarvis, L. E.; Langridge, R. *J. Mol. Graphics* **1988**, *6*, 13−27.
(27) Huang, C. C.; Pettersen, E. F.; Klein, T. E.; Ferrin, T. E.; Langridge, R. *J. Mol. Graphics* **1991**, *9*, 230−236.
(28) Shriver-Lake, L. C.; Patterson, C. H.; van Bergen, S. K. *Field Anal. Chem. Technol.* **2000**, *4*, 239−245.
(29) Goldman, E. R.; Cohill, T. J.; Patterson, C. H.; Anderson, G. P.; Kusterbeck, A. W.; Mauro, J. M. *Environ. Sci. Technol.* **2003**, *37*, 4733−4736.

of TNB2-45 at 639 nM, QDs at 36.5 nM, and TNB−BHQ-10 at 1.26 μM) were mixed with equal volumes (50 μL) of unknown sample in the wells of a microtiter plate, and fluorescence intensity was collected. Known dilutions of TNT standards were run on the same plate to facilitate construction of a standard curve for quantification of TNT derived from the soil samples.

Results and Discussion

QD−Protein Conjugation. We have previously shown that oligohistidine-appended proteins can self-assemble on DHLA-capped CdSe−ZnS core−shell QDs via metal-affinity coordination.[14,15,23] We have also derived a FRET-based structural model for these QD−protein nanoassemblies and shown that a polyhistidine tail in proximity to the QD surface is necessary to facilitate this process.[30] The coordination of oligohistidine-appended proteins to Zn ions on the QD surface is anticipated to yield an equilibrium dissociation constant equivalent to or stronger than most antibody−antigen interactions ($K_D > 10^{-9}$).[31] The anti-TNT scFv fragment used in this study, TNB2-45, has already been shown to coordinate to QDs and produced QD reagents that functioned in a displacement fluoroimmunoassay targeting soluble TNT.[23]

Steady-State FRET Quenching Assays. Figure 2C shows the QD PL spectra for 530 nm emitting nanocrystals at increasing amounts of added TNB−BHQ-10 (reported as dye-labeled analogue to QD ratio, *n*) collected from two series of wells: one set containing QD−TNB2-45 conjugates and the other QDs conjugated to apo-myoglobin. Spectra collected from experiments using 555 and 570 nm emitting nanocrystals showed similar behavior. Figure 2D shows the PL integrated intensity versus TNB−BHQ-10 to QD ratio for the three populations of QDs used: 530, 555, and 570 nm emitting nanocrystals. The data clearly show that as the TNB−BHQ-10 to QD ratio was increased in the set of wells containing QD−anti-TNT scFv assemblies, the QD PL progressively decreased in a systematic and concentration-dependent manner, with an estimated loss of about 55−60%, measured for the three color QDs used when the TNB−BHQ-10 to QD ratio reached ∼32 (which corresponds to a TNB−BHQ-10 to TNB2-45 ratio of ∼2). When the TNB−BHQ-10 reagent was added to wells containing QD−apo-myoglobin conjugates, only a small PL change was measured, with a maximum loss of ∼5%, measured for the TNB−BHQ-10 to QD ratio of ∼32 (see Figure 2). Increasing the TNB−BHQ-10 concentration (beyond a BHQ-10 to QD ratio of ∼32) resulted in further decrease in the QD PL signal in both cases. At a BHQ-10 to QD ratio of ∼128 (TNB−BHQ-10 to protein ratio of ∼8), we measured ∼30% loss of PL for the apo-myoglobin conjugated QDs, whereas that loss reached 80% in the case of QDs conjugated to TNB2-45.

The above set of data, namely, the pronounced and concentration-dependent loss of QD PL in the presence of increasing amounts of quencher−analogue complexes, occurs only when QD−TNB2-45 conjugates were used (see Figure 2), which results from the capture of TNB−BHQ-10 by the anti-TNT scFv in the QD conjugates. This capture brings the quencher in proximity of the QD donor, resulting in an efficient and progressive FRET quenching of the QD PL signal, reaching about 60% for a quencher to QD ratio of ∼32. This contrasts

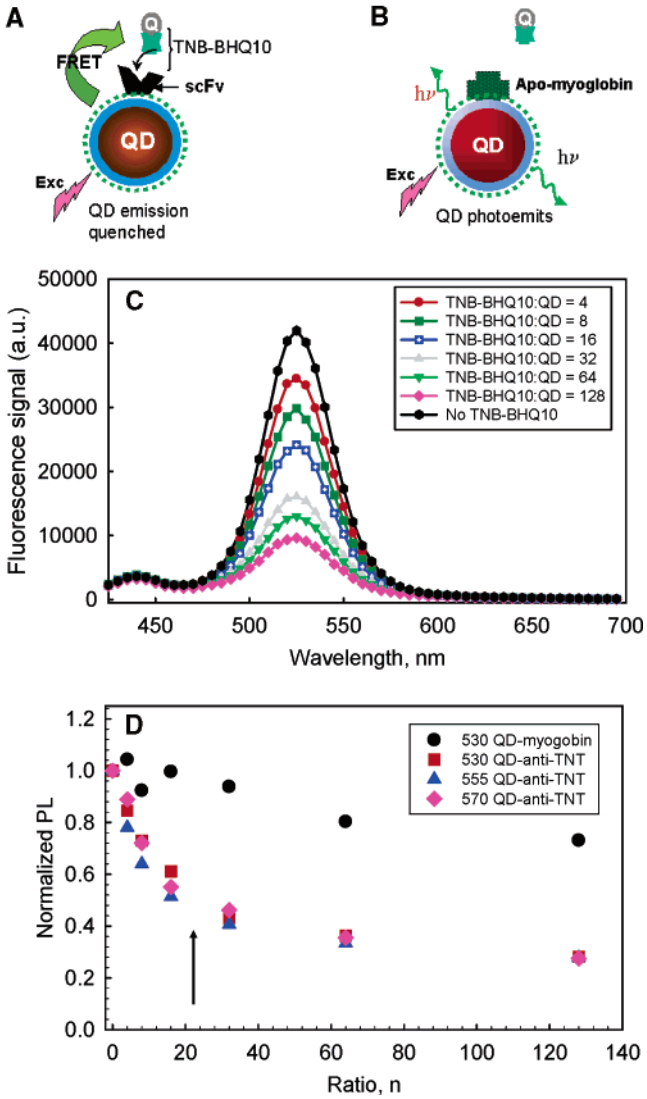

Figure 2. Addition of TNB−BHQ-10 to QD−protein assemblies constructed with apo-myoglobin and with the TNB2-45−anti-TNT antibody fragment. Schematic diagrams showing the QD−TNB2-45 conjugate interacting and binding with the BHQ-10-labeled analogue (A) and QD−apo-myoglobin conjugate, which has no specific interactions with the quencher analogue (B). For simplicity, only one protein per QD is shown. (C) PL spectra of the 530 nm emitting QD−TNB2-45 conjugates as a function of increasing quencher-labeled analogue to QD ratio. TNB−BHQ-10 bound to the TNB2-45 is in proximity to the QD, which induces concentration-dependent FRET quenching of the QD fluorescence. (D) Integrated PL intensity of the QDs versus BHQ-10 to QD ratio *n* for the three sets of QD−TNB2-45 conjugates used along with a typical set of data for a 530 nm QDs conjugated to apo-myoglobin. Curves shown are the average of three measurements. The arrow designates the transition from a range where the ratio of analogue to conjugated protein is smaller than 1 to a region where that ratio exceeds 1. For ratios below 1, quenching of QD emission is systematic and concentration-dependent in the presence of QD−anti-TNT conjugates, but only minimal decrease in the emission is measured when apo-myoglobin is assembled on the nanocrystal. At higher ratios, nonspecific interactions with apo-myoglobin start to contribute to the measured decrease in the donor PL.

with the case where the quencher-labeled analogue is added to solutions containing QD−apo-myoglobin, where no specific interactions exist and primarily solution-induced FRET estimated at ∼5−7% loss (possibly coupled with some degree of nonspecific interactions) could be measured. Analysis of the solution-induced FRET data was carried out using a Stern−Volmer analysis (see Supporting Information). The slightly

(30) Medintz, I. L.; Konnert, J. H.; Clapp, A. R.; Stanish, I.; Twigg, M. E.; Mattoussi, H.; Mauro, J. M.; Deschamps, J. R. *Proc. Natl. Acad. Sci. U.S.A.* **2004**, *101*, 9612−9617.

larger PL loss measured at higher concentration (30% at TNB−BHQ-10 to apo-myoglobin ratio of 8 or TNB−BHQ-10 to QD of 128) is most likely due to more pronounced nonspecific interactions of the analogue with apo-myoglobin. The PL loss reached ~80% with QD−TNB2-45 conjugates.

Our present quenching assays utilized an analog quencher to antibody fragment ratio of 2 (BHQ-10 to QD ratio of ~32) to induce a PL loss of 60% nearly all of which can be attributed to FRET. It contrasts with our previous QD−MBP FRET quenching prototype, where the amount of dye-labeled analogue added to induce similar efficiencies was in 10-fold excess of the MBP concentration.[15] This is probably a result of the very different structure of the scFv versus that of MBP as well as the difference in strength between the interactions of scFv with the TNB target and those between MBP and cyclodextran (analogue used with maltose).

Nonradiative Förster energy transfer is highly dependent on the distance between the donor and acceptor fluorophores.[32] Furthermore, in a configuration where a single exciton donor is made to interact with several acceptors, the rate of FRET (E) depends on the acceptor to donor molar ratio and can be expressed as[14]

$$E = \frac{nR_0^{\,6}}{nR_0^{\,6} + r^6} \qquad (1)$$

where n designates the number of acceptors interacting with a single donor for a centro-symmetric system with equal separation distance, r, from the donor center to all acceptors, such as a QD−protein conjugate. R_0 is the Förster distance at which the FRET efficiency is estimated at 50%; it is defined as[14,32]

$$R_0 = (BQ_D I)^{1/6} = \left(\frac{9000(\ln 10)\kappa_p^{\,2} Q_D}{N_A 128\pi^5 n_D^{\,4}} I\right)^{1/6} \qquad (2)$$

where Q_D is the quantum yield of the donor, and I is the integral of the spectral overlap between acceptor absorption and donor emission (see Figure 1); the constant B is a function of Avogadro's number, N_A, the refractive index of the medium, n_D, and a parameter, κ_p, that depends on the relative orientation of the donor and acceptor dipoles.[14,32] We used $\kappa_p^{\,2} = {}^2/_3$ for randomly oriented dipoles.[14,15]

The R_0 values for the present QD−BHQ-10 pairs are modest compared with those in the case of Cy3−dye acceptors, a feature primarily due to the rather low extinction coefficient of the BHQ-10 quencher (30 000 M^{-1} cm^{-1} compared with 150 000 M^{-1} cm^{-1} for Cy3). This translates into a more modest rate of FRET than what was measured previously for the QD−Cy3 pair. Nonetheless, the ability to array several acceptors around a single donor compensates for this modest energy overlap and enhances the overall FRET efficiencies measured, as shown in Figure 2.[14,15]

A fit of the experimental data for the FRET efficiency using eq 1 but limited to n values of 4, 8, and 16 provided an estimate for the separation distance (r) between the QD center and the acceptor for the three sets of QD donors: ~71 ± 1, ~72 ± 1, and ~71 ± 3 Å for the 530, 555, and 570 nm emitting QDs, respectively. Using these values, we generated prediction curves for the FRET efficiency expected from the Förster formalism (eq 1) for the full range of ratios (n) explored (Figure 3). The predicted FRET quenching (and thus efficiency) expected for the higher TNB−BHQ-10 concentrations (n = 32, 64, 128) is ~10 and 15% larger than what was experimentally measured (see Figure 3). This implies that increasing the number of quenchers in the solution translated to a measurable increase of only ~7−10% additional FRET, which can be attributed to solution-induced FRET. This is expected since the extra TNB−BHQ-10 added cannot be captured by the anti-TNT scFv on

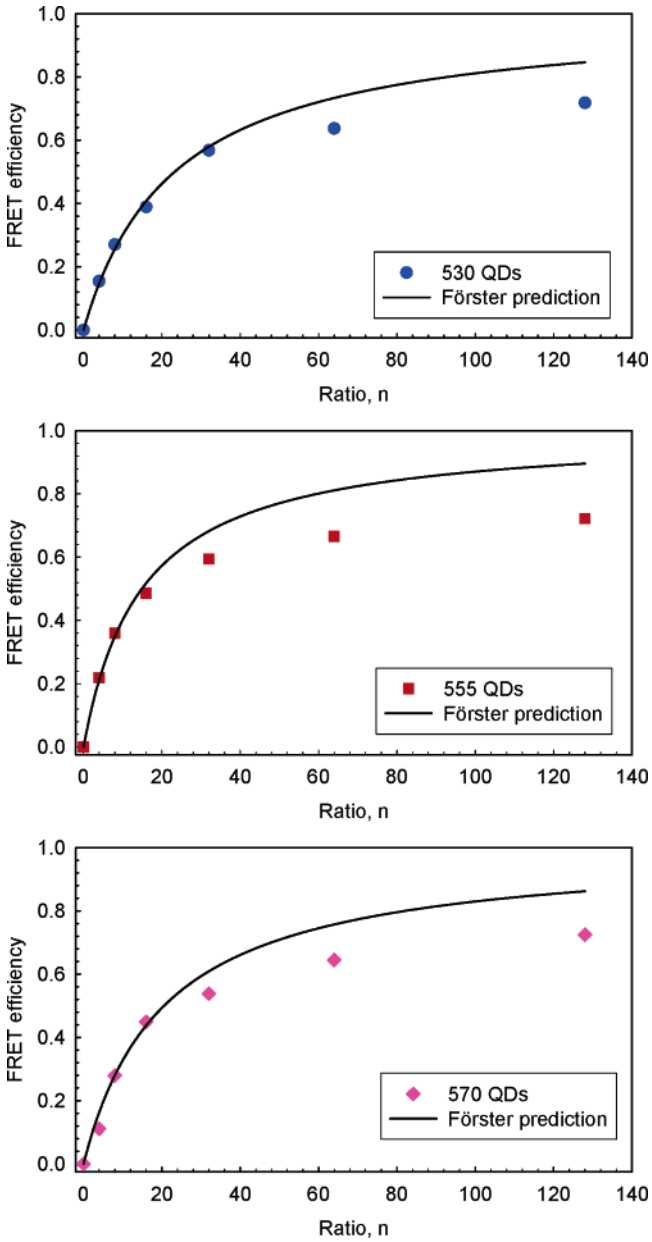

Figure 3. Comparison of experimental FRET efficiencies (derived from the data in Figure 2C and D) and the prediction derived from eq 1 using the experimental values for R_0 and the distance r extracted for the data at low n[4,8,16]; both are plotted versus ratio n for the three sets of QDs used. At higher n, the predictions exceed the experimental efficiencies, a feature attributed to a lack of proximity-induced FRET when the number of quencher analogues becomes larger than the number of available sites (anti-TNT) in each conjugate.

(31) Hainfeld, J. F.; Liu, W. Q.; Halsey, C. M. R.; Freimuth, P.; Powell, R. D. *J. Struct. Biol.* **1999**, *127*, 185−198.
(32) Lakowicz, J. R. *Principles of Fluorescence Spectroscopy*; Kluwer Academic/Plenum Publishers: New York, 1999.

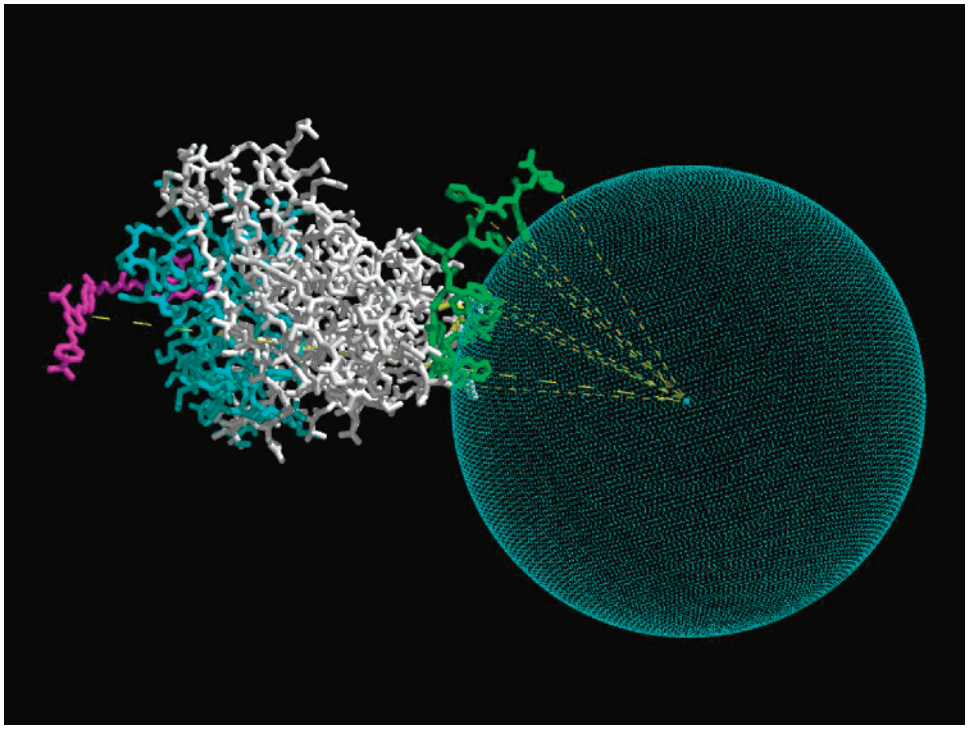

Figure 4. Structural model showing TNB−BHQ-10 bound by TNB2-45 conjugated to a QD. The C-terminal attachment point is yellow; the poly-His tail is green; the "binding region" (as defined by the variable regions of the scFv) is cyan; the TNB−BHQ-10 complex is magenta. In this view, the distance between the QD center and the TNB−BHQ-10 is 72 Å and five of the His residues are in close contact with the QD.

the QDs and thus would not contribute to the FRET quenching caused by docking of the analogue in the antibody binding site. They would contribute through diffusion-induced proximity to the QD−TNB2-45 conjugate, thus resulting in a weaker increase in the measured rate of energy transfer.

Using the above estimate for the donor−acceptor separation distance and the QD finite radii extracted from size measurements using transmission electron microscopy (TEM) and scattering techniques,[16,18,34] we infer a distance between the His tail at the QD surface and the dye-labeled analogue docked in the anti-TNT binding pocket of ∼40−43 Å. This value accounts for the anti-TNT fragment's spatial extension away from the QD surface together with the TNB−BHQ-10 complex.

Indeed, modeling of the TNB-45 conformation on the surface of the QD shows that this is a reasonable estimate of the donor−acceptor separation (Figure 4). The TNB−BHQ-10 complex was docked in the binding region of a model scFv based on $\pi-\pi$ interaction between TNB and a tryptophan (Trp) side chain. The conformation of the histidine-rich tail was adjusted to allow for coordination between this region and the QD surface. This is a necessary assumption, as close interactions between the histidine residues and the nanocrystal surface are required to allow for the conjugate to self-assemble, as shown in our prior studies modeling the optimal conformation of maltose binding protein on the QDs.[30] In that investigation, we found that a close approach of the C-terminal oligohistidine tail to the QD surface is required for the QD−MBP to assemble based on a molecular orientation derived from multiple FRET measurements.[30] In this model, the distance between the QD center and the TNB−BHQ-10 is ∼72−74 Å, with residues from both the first and second $(His)_6$ interacting with the QD surface. The conformation shown in Figure 4 was derived from the best agreement between the experimentally measured donor-to-acceptor distance and the necessary proximity of the histidine side chains to the QD surface. Alternate conformations for the model (including a fully extended histidine tail) result in distances between the QD center and the TNB−BHQ-10 ranging from about 65 to 120 Å.

Sensor Function and Determination of TNT Concentration. We examined the ability of the QD−TNB2-45 conjugates to detect soluble TNT. Starting from samples made of QD−TNB2-45 conjugates pre-assembled with TNB−BHQ-10, the fluorescence was monitored upon addition of TNT at increasing concentration. Figure 5 shows a typical experiment examining changes in the PL intensity of 570 nm emitting QDs (reported as the increase relative to the case of a TNB−BHQ-10 to QD ratio of ∼32) with increasing concentrations of added TNT. Similar results were measured for the other QD donors (530 and 555 nm emitting nanocrystals). The data show a systematic recovery of the donor PL signal with increasing TNT concentration, indicating a progressive concentration-dependent loss of FRET between the QD and the TNB−BHQ-10 as the target analyte concentration was increased. These results prove that the added soluble TNT displaced the analogue quencher away from the antibody, reducing the rate of FRET, which indicates the ability of our designed QD−anti-TNT assembly to function as an effective sensor based on FRET. Within the range of examined TNT concentrations (9.8 ng/mL to 10 μg/mL), the lowest value that produced a measurable signal recovery was 20 ng/mL. The QD signal recovery followed a very pronounced nonlinear dependence on the TNT concentrations, with most of the changes occurring in the window between 0 and 0.5 μg/mL. At higher concentrations (i.e., between 0.3 and 10 μg/mL of TNT), the PL increase followed a logarithmic dependence on the TNT concentration, as shown by the linear response when plotted against the log of the concentration. The PL response of the sensor was well described by a four-parameter Hill

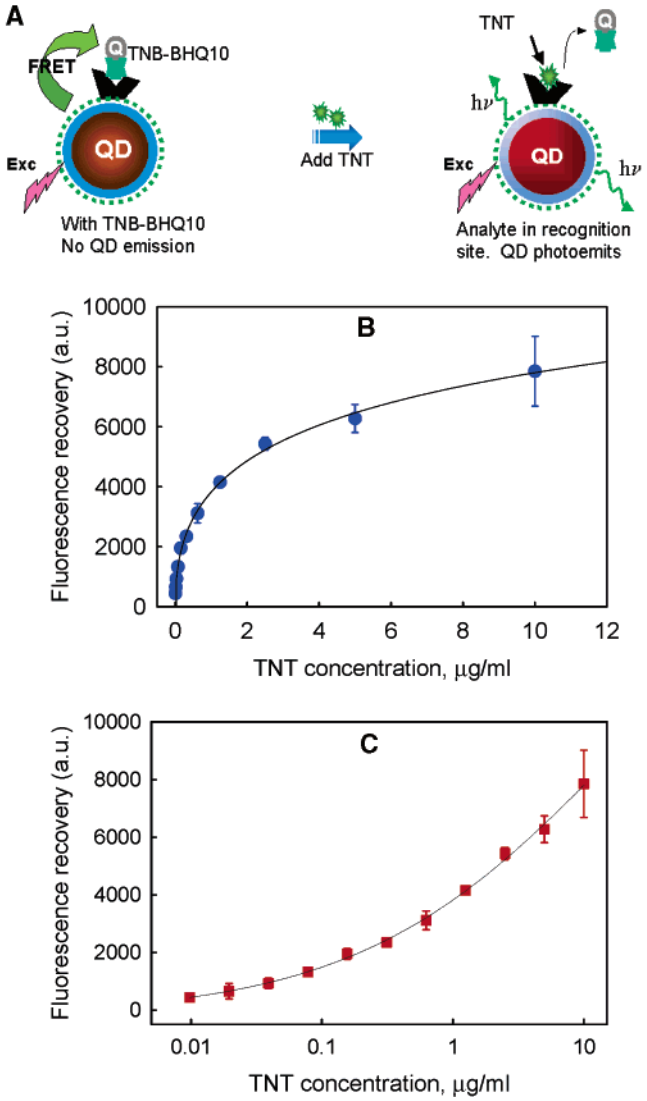

Figure 5. TNT titration of QD−TNB2-45 nanosensor assembly. (A) Schematic of the assay. When TNB−BHQ-10 is bound to the QD−TNB2-45 conjugate, QD fluorescence is quenched. As TNT is added to the assay, it competes for binding to the antibody fragment and the QD fluorescence increases following TNB−BHQ-10 release from the conjugate. The data resulting from the increase in QD PL are plotted as the difference signal versus concentration, both in linear (B) and logarithmic (C) scales. The assembly in (B and C) was constructed using 570 nm emitting QDs. Each data point is an average of three measurements, and error bars represent the standard deviation. The data were fit to a four-parameter Hill function (solid lines) appropriate for describing binding equilibria. On the basis of the fit, the measured dissociation constant, K_D, for this system was 15.7 μM.

function of the type: $y(x) = y_0 + ax^b/(c^b + x^b)$, where a, b, and c are fitting parameters.[32] A K_D value corresponding to 50% saturation of ~15.7 μM was derived for the present system.

Our present conjugate assembly was also tested for the detection of TNT dissolved in artificial seawater. We observed FRET-induced quenching in the presence of TNB−BHQ-10 and a systematic concentration-dependent PL recovery upon adding increasing concentrations of TNT, indicating the ability of our sensing assembly to function in seawater (see Supporting Information).

In addition to the donor−acceptor distance, FRET is dependent on spectral overlap between the emission spectra of the donor and the absorption spectra of the acceptor. We performed TNT titrations using three different size QDs (emitting at 530, 555, and 570 nm) and produced PL recovery curves showing essentially identical behavior with the three QD populations. These results demonstrate that within a certain range of QD size and hence QD emission, efficient FRET sensing can be achieved. This can be attributed to a combination of small size of TNB2-45 (MW about 27 kD) and the broad absorption spectrum of the dye, which together allows the TNB−BHQ-10 to be well within the Förster distance of all three QDs used. In future sensor designs, utilizing larger biorecognition elements along with a different dye analogue, critical Förster distances may come into play; the ability to size tune the QD emission will thus become more critical to sensor function.

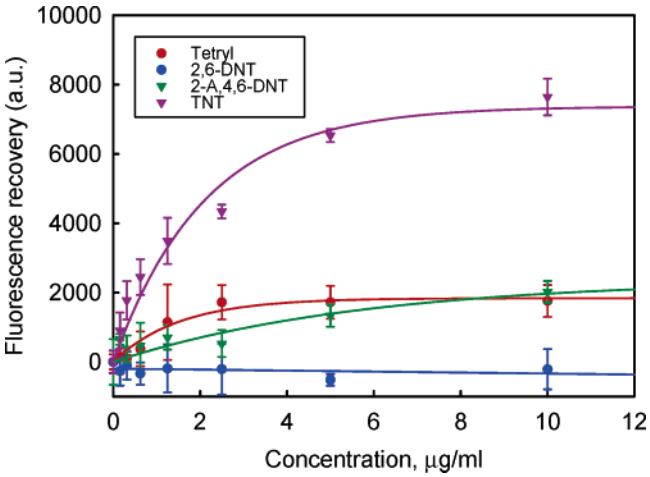

Figure 6. Results from titration of the QD−TNB2-45−TNB−BHQ-10 assembly with TNT and the indicated TNT analogues. These assemblies were constructed using 530 nm emitting QDs. Each data point is an average of three measurements, and error bars represent the standard deviation. Solid lines are guides to the eye drawn through the experimental points.

In addition to employing the TNB−BHQ-10 quencher, we examined the use of a TNT analogue bound to a fluorescent dye (AlexaFluor555) as the energy acceptor in these assays. We achieved the same sensing range using a TNB−DAP−AlexaFluor555 in the sensor assembly (data not shown). Using a quencher rather than an emissive fluorophore as an acceptor is more desirable as the sensor functions in a "switch on mode".[30]

Sensor Specificity. Specificity of the present QD-based sensing assembly was investigated by monitoring the loss of FRET as three TNT analogues (Tetryl, 2-A,4,6-DNT, and 2,6-DNT) were added to the sensor solution. Figure 6 shows a side-by-side comparison of the QD PL recovery with increasing concentration of TNT analogues added to the QD conjugate pre-assembled with TNB−BHQ-10, together with the recovery signal induced by TNT. Signal recovery was small (at least ~4 times smaller) for Tetryl and 2-A,4,6-DNT and negligible in the presence of 2,6-DNT. The responses elicited by our FRET-based QD assembly are similar to those measured for the antibody fragment in competitive immunoassays described in ref 22. This indicates that the specificity observed for the QD−TNB2-45 nanosensor is essentially the same as that of the antibody fragment, with a moderate crossreactivity elicited with Tetryl and 2-A,4,6 DNT and essentially none with 2,6-DNT. These results overall demonstrate that attaching the antibody fragment to the QD surface via noncovalent self-assembly did not alter the antibody specificity through any allosteric effects.

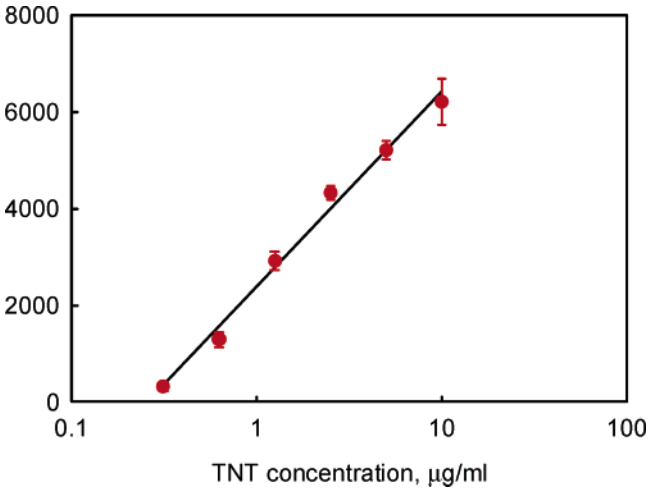

Figure 7. Curve constructed from titration of QD−TNB2-45−TNB−BHQ-10 nanosensor assembly with a TNT standard. These dilutions were run on the same microwell plate at the same time as dilutions derived from contaminated soil samples to extract the values shown in Table 1. Assemblies used in this experiment were constructed using 530 nm emitting QDs. Each data point is an average of three measurements, and error bars represent the standard deviation.

These observations confirm our prior findings with the prototype solution-phase QD−MBP sensor assembly where we showed that surface-immobilized maltose binding proteins maintained their affinity and specificity toward their maltose substrate.[15]

Analysis of Soil Samples. The QD-based TNT sensor was applied to samples of contaminated soil to estimate the TNT concentration in these media. The TNT was extracted from the soil as described in the Experimental Section. TNT standard solutions were tested side-by-side with the unknown counterparts, and focusing on the linear regime of PL changes versus concentration (reported in logarithmic scale) permitted the construction of a "standard" curve to which our data were compared (Figure 7). From this curve and the fluorescence recovery measured for the unknown samples, we were able to derive estimates of TNT levels in the acetone extracts collected from contaminated soil samples. A summary of the calculated mean TNT concentration for each soil extract from the FRET assay and the corresponding result from HPLC analysis of the same samples is shown in Table 1. The values determined by the FRET assay follow the same trend as those found by HPLC, showing the ability of our QD−scFv sensing assembly to provide accurate measures of TNT concentrations in unknown environmental samples.

Conclusions

We have demonstrated the use of a solution-phase hybrid QD−antibody fragment nanosensor based on FRET specific for the detection of the explosive TNT, a security threat and environmental contaminant. The nanosensor was built by self-assembling single-chain antibody fragments onto luminescent CdSe−ZnS core−shell QD fluorophores, via metal-affinity coordination, to form compact QD−anti-TNT conjugates compatible with FRET interactions/processes. This conjugate produced a substantial rate of FRET when pre-assembled with a quencher-labeled TNT analogue. Further, using an acceptor with a broad absorption spectrum allowed the use three size (color) QD donors and achieved high rates of FRET in all cases. Analysis of the FRET data provided an estimate of the antibody fragment size and insight into how it self-assembles on the QD surface. Exposure to soluble TNT produced a systematic and concentration-dependent QD PL recovery, due to displacement of the analogue quencher away from the QD−TNB2-45 conjugate. Potentially, more sensitive detection using our QD-based FRET sensing format can be achieved through further protein engineering and optimization to produce anti-TNT scFvs with higher affinity and specificity toward TNT.

Table 1. TNT Concentrations Determined for Acetone Extracts of Soil Using FRET and HPLC Analysis[a]

soil sample	FRET assay (mg/L)[b]	HPLC (mg/L)[b]
G16-L2A	7.9 ± 3.0	9.9 ± 0.6
G18-L1-A	9.5 ± 2.9	15.6 ± 0.6
G55-X−A	62 ± 30	153 ± 0.7

[a] Values shown are the calculated mean TNT concentration for each soil extract and were determined from three replicates. [b] Concentration of TNT in acetone extracts.

The unique spectral properties of QDs should eventually allow for the simultaneous FRET-based monitoring of multiple environmental contaminants using a single well of a microtiter plate or a flow cell. Indeed, we have realized multiplex format in a four-color QD-based fluoroimmunoassay to detect four toxin proteins simultaneously.[35] The requirements for future sensor design and construction using the current scheme include access to small recognition elements such that the overall size does not constrain the FRET process (antibody fragments versus whole antibodies) as well as the construction of an appropriate dye analogue of the target analyte or contaminant. The choice of recognition element will dictate the sensitivity and specificity of such sensors.

Acknowledgment. The authors acknowledge NRL, A. Ervin, and K. Ward at the Office of Naval Research for the financial support, ONR Grant N001404WX20270. We also thank A. Krishnan at DARPA for financial support. A.H. was partially funded by a grant from the USAA foundation, a charitable trust and NIH C06RR12087. I.L.M., A.R.C., and H.T.U. were supported by National Research Council Fellowships through NRL. M.E.L. is supported by an American Society for Engineering Education (ASEE) fellowship.

Supporting Information Available: Figure showing TNT titration of QD−TNB2-45−TNB−BHQ-10 nanosensor assembly constructed using 550 nm emitting QDs in both borate buffer and artificial seawater. Analysis of apo-myoglobin conjugate data in Figure 2D using the Stern−Volmer model. This material is available free of charge via the Internet at http://pubs.acs.org.

JA043677L

(33) De Lorimier, R. M.; Smith, J. J.; Dwyer, M. A.; Looger, L. L.; Sali, K. M.; Paavola, C. D.; Rizk, S. S.; Sadigov, S.; Conrad, D. W.; Loew, L.; Hellinga, H. W. *Protein Sci.* **2002**, *11*, 2655−2675.
(34) Mattoussi, H.; Cumming, A. W.; Murray, C. B.; Bawendi, M. G.; Ober, R. *Phys. Rev. B* **1998**, *58*, 7850−7863.
(35) Goldman, E. R.; Clapp, A. R.; Anderson, G. P.; Uyeda, H. T.; Mauro, J. M.; Medintz, I. L.; Mattoussi, H. *Anal. Chem.* **2004**, *76*, 684−688.